The 8 January 2006 Earthquake (M_w 6.7) Offshore Kythira Island, Southern Greece: Seismological, Strong-motion, and Macroseismic Observations of an Intermediate-depth Event

Konstantinos I. Konstantinou, Ioannis S. Kalogeras, Nikolaos S. Melis, Moissis C. Kourouzidis, and George N. Stavrakakis
Institute of Geodynamics, National Observatory of Athens

INTRODUCTION

On 8 January 2006 at 11:34 GMT (13:34 local time), a strong earthquake with a moment magnitude of 6.7 occurred in southern Greece, off the eastern coast of the island of Kythira. The epicentral coordinates as estimated by the European Mediterranean Seismological Centre (EMSC-CSEM, http://emsc-csem.org were 36.31°N, 23.24°E, and the focal depth was 60 km. The shock was felt in a spatially extended area that covered Greece, Italy, Turkey, Egypt, Cyprus, Israel, Syria, Jordan, and Lebanon. Despite the large magnitude of the earthquake, the reported damage was not extensive mainly due to the intermediate focal depth. No casualties were reported and the structural damage to buildings was limited to the islands of Kythira and Antikythira and to the city of Chania, western Crete. Furthermore, landslides and/or rockfalls were reported only at the village of Mitata (Kythira island), where the main square and the road were damaged due to a landslide.

Intermediate-depth earthquakes in this region are related to the southern Aegean subduction zone, which is referred to as the Hellenic arc (figure 1). The deformation that takes place along this arc is caused by the motion and collision of the southern part of the Eurasian plate with the African plate at a rate of 40–60 mm/year. The basic picture of the regional kinematics has not changed much since the early work of McKenzie (1972, 1978) but has been studied in more detail recently using GPS data (LePichon *et al.* 1995; McClusky *et al.* 2000; Nyst and Thatcher 2004, among others). The continuation of the Hellenic arc is interrupted by active fault zones with a perpendicular orientation relative to the boundary of the two plates (Lyberis *et al.* 1982). One of these structures exists in the vicinity of Kythira island and during the 20th century produced five strong earthquakes: in 1903 (*M* 7.5), 1910 (*M* 7.0), 1926 (*M* 7.2), 1937 (*M* 6.0), and 1932 (*M* 6.2) (Papazachos and Papazachou 1997).

In this article we take advantage of a multitude of available observations to give a detailed report on this most recent large intermediate-depth earthquake. First, we describe the temporal and spatial distribution of the mainshock-aftershock sequence and summarize all available moment tensor solutions reported by various agencies. Then, we present preliminary analysis of strong-motion recordings in an effort to check the relationship between the shaking caused by such an event and the influence of both attenuation and local geological conditions. Macroseismic data collected from the whole of Greece also are included and utilized toward understanding the regional intensity attenuation pattern. Finally, we give an overview of the implications of such an event in terms of regional seismotectonics and seismic hazard.

SEISMOLOGICAL OBSERVATIONS

The National Observatory of Athens, Institute of Geodynamics (NOAIG) is responsible for the operation of the Greek national seismic network (also known as the HL network, http://bbnet.gein.noa.gr) and the monitoring of earthquake activity in the country (figure 2). The network consists of 22 stations equipped with broadband (up to 20–30 s) three-component seismometers recording continuously at a sampling interval of 50 samples per second. An additional seven stations are equipped with broadband instruments (up to 120 s) operated by the GEOFON and MEDNET groups in collaboration with NOAIG. The data are transferred via dedicated telephone lines in near real-time to a collection center in Athens where they are stored for further analysis. This includes phase picking, location, and local magnitude determination and, in cases when the earthquake is larger than M_L ~4, inversion of the broadband waveforms for moment tensor derivation. A detailed description of the network operation and near real-time data processing can be found in Melis and Konstantinou (2006).

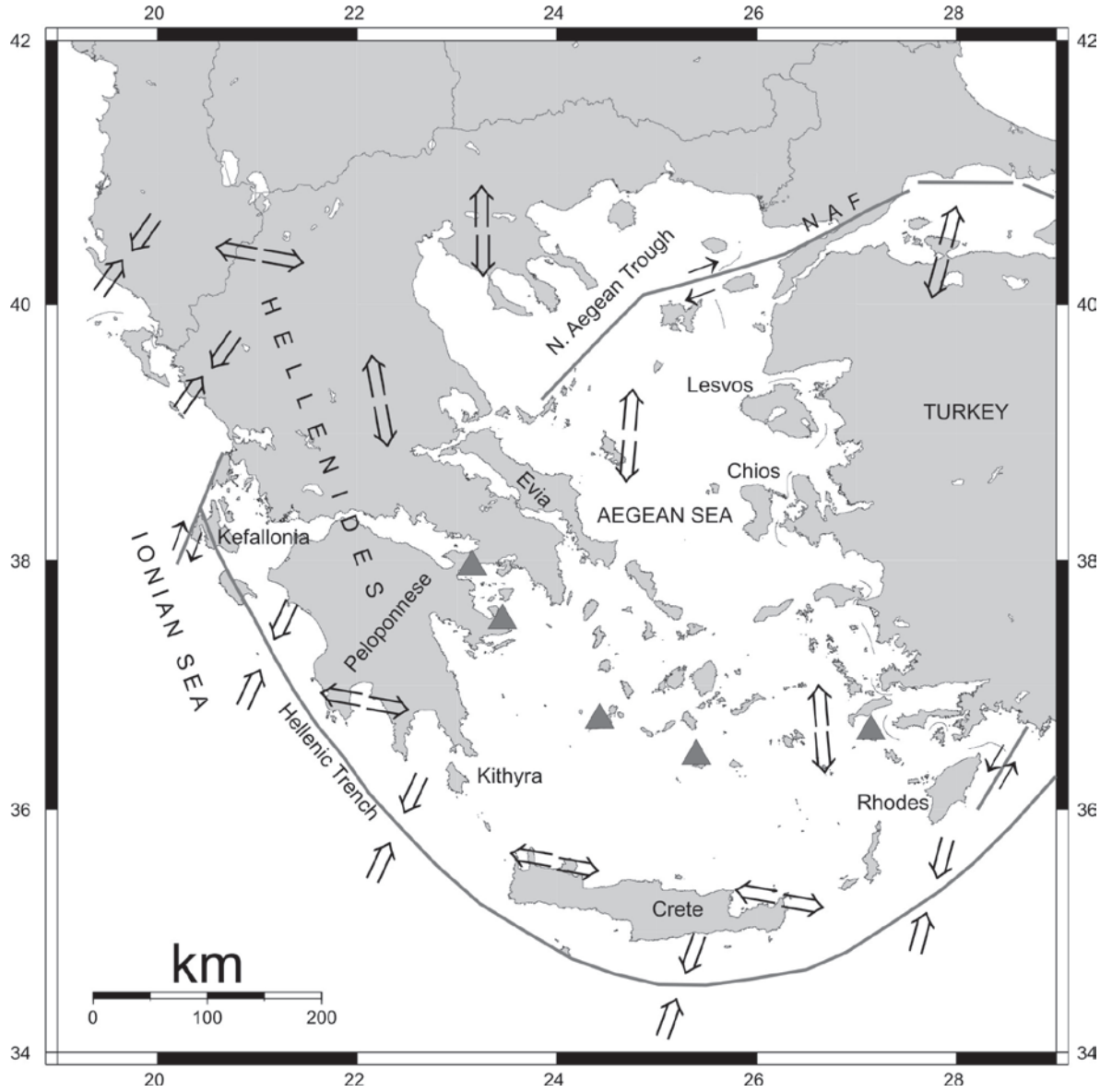

▲ **Figure 1.** Main features of tectonic region in the broader Aegean region. Triangles represent volcanic centers and open arrows represent the stress regime (compressional, extensional, strike slip). NAF: North Anatolian Fault.

The mainshock as well as several of its aftershocks were recorded by the HL network, and our analysis started by manually picking *P*- and *S*-phase arrival times of these events for the period between 8 January 2006 and 20 May 2006. These arrival times subsequently were inverted using HYPO2000 (Klein 2002) assuming a velocity model and V_P / V_S ratio of 1.78 based on the results of the tomographic study for the Aegean Sea region published by Papazachos and Nolet (1997) (table 1). The inferred mainshock location (36.21°N, 23.42°E, 65 km) appears to be consistent with the one reported by EMSC-CSEM (the difference between the two locations is 19 km). Figure 3 shows the locations that exhibit formal errors in the horizontal (ERH) and vertical (ERZ) directions smaller than 4 km and rms residuals smaller than 1 s. Most aftershocks occur at depths shallower than the mainshock, while the orientation of the epicenter cluster is roughly NE–SW.

Several institutes/agencies have reported moment-tensor solutions for the mainshock using either teleseismic (Harvard CMT, USGS, CPPT) or regional (ETH, INGV, AUTH) waveform data (figure 3). All of these solutions exhibit a predominantly reverse slip component, even though the exact fault strike varies among the reported mechanisms from E–W to NE–SW. This perpendicular/oblique direction to the trench also is consistent with the orientation of the epicentral locations reported earlier. Waveform data recorded by the HL network also were inverted for the purpose of deriving moment-tensor solutions for the mainshock and two of its largest aftershocks (see NOAIG solutions in figure 3). The inversion methodology follows that of Randall *et al.* (1995) and also is described by Melis and Konstantinou (2006). It should be noted that the closest HL stations to the epicenter were clipped; therefore only stations at distances greater than 100 km were used in the inver-

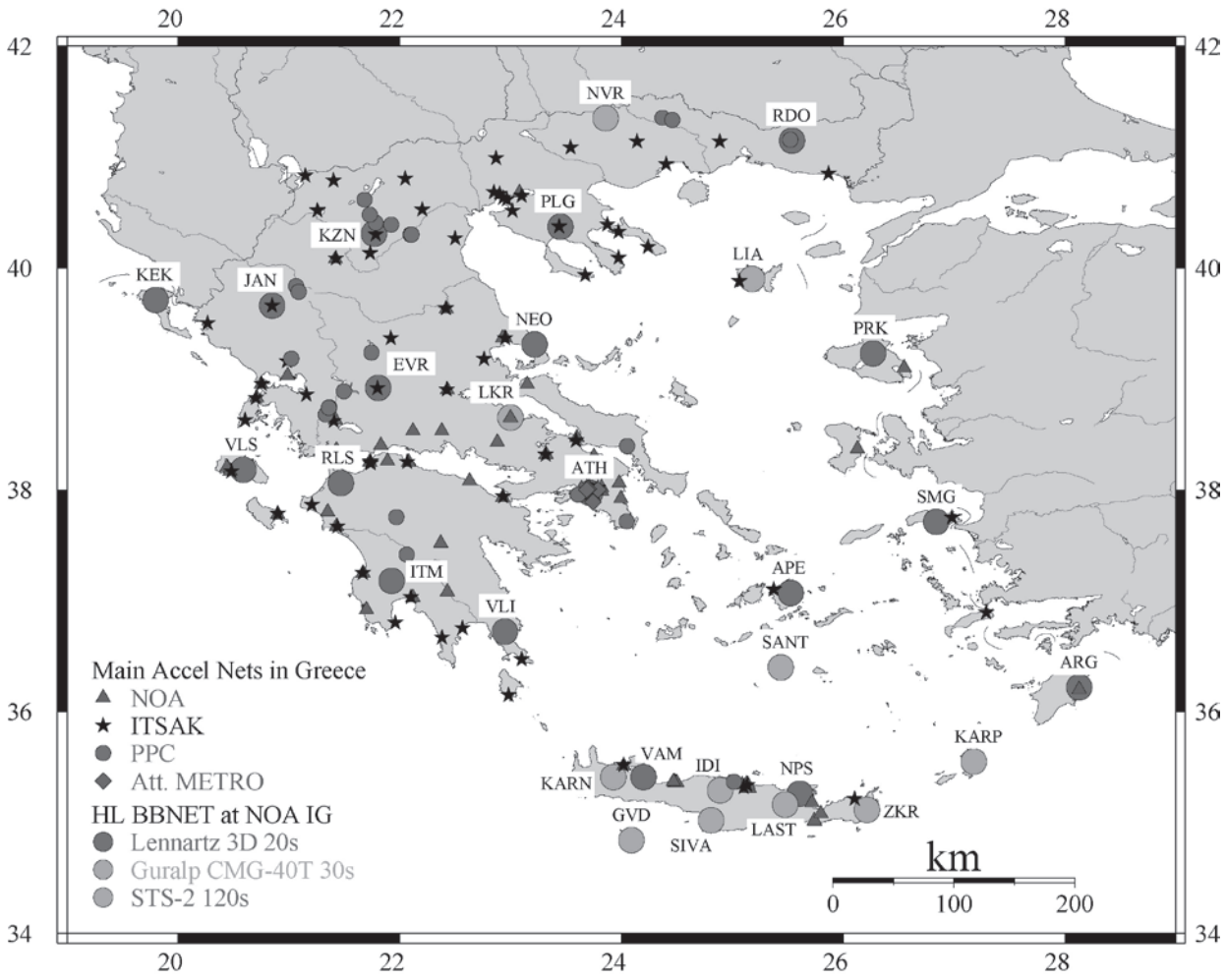

▲ **Figure 2.** Map showing station locations of broadband three-component seismometers and available strong ground motion instruments in the Greek region.

sion process (for details see the HL Web page, http://bbnet.gein.noa.gr). The mainshock solution appears similar to those referred to previously, exhibiting a purely reverse slip motion with the fault orientation striking perpendicular to the trench. The two aftershock focal mechanisms also exhibit reverse slip motion even though the strike for one solution is rotated clockwise with respect to that of the mainshock. Table 2 summarizes all information for the available moment tensor solutions shown in this study.

STRONG MOTION OBSERVATIONS

NOAIG also operates a network of strong-motion instruments at a national scale, as well as a local array in the broader area of Athens in cooperation with Attiko Metro S.A., the Athens subway company. The advantages of the operation of this local array were apparent during the 7 September 1999 (M_w 5.9) Athens earthquake: It produced more than 300 recordings that were used to construct a strong-motion database for the Athens metropolitan area (Kalogeras and Stavrakakis 2001). A number of additional strong-motion instruments are installed at dams and thermoelectric stations and are operated by the Public Power Corporation (PPC). Furthermore, the Institute of Earthquake Engineering and Engineering Seismology (ITSAK, http://www.itsak.gr) operates its own strong-motion instrument network, and its reported peak ground acceleration (PGA) values (Karakostas *et al.* 2006), also were incorporated in this study. Figure 2 shows the locations of all these strong-motion instruments.

TABLE 1
***P*-velocity model after Papazachos and Nolet (1997), which was used for intermediate depth earthquake location**

***P*-velocity (km/s)**	**Crustal Depth (km)**
6.00	19
6.60	31
7.90	50
7.95	100
8.00	120
8.05	∞

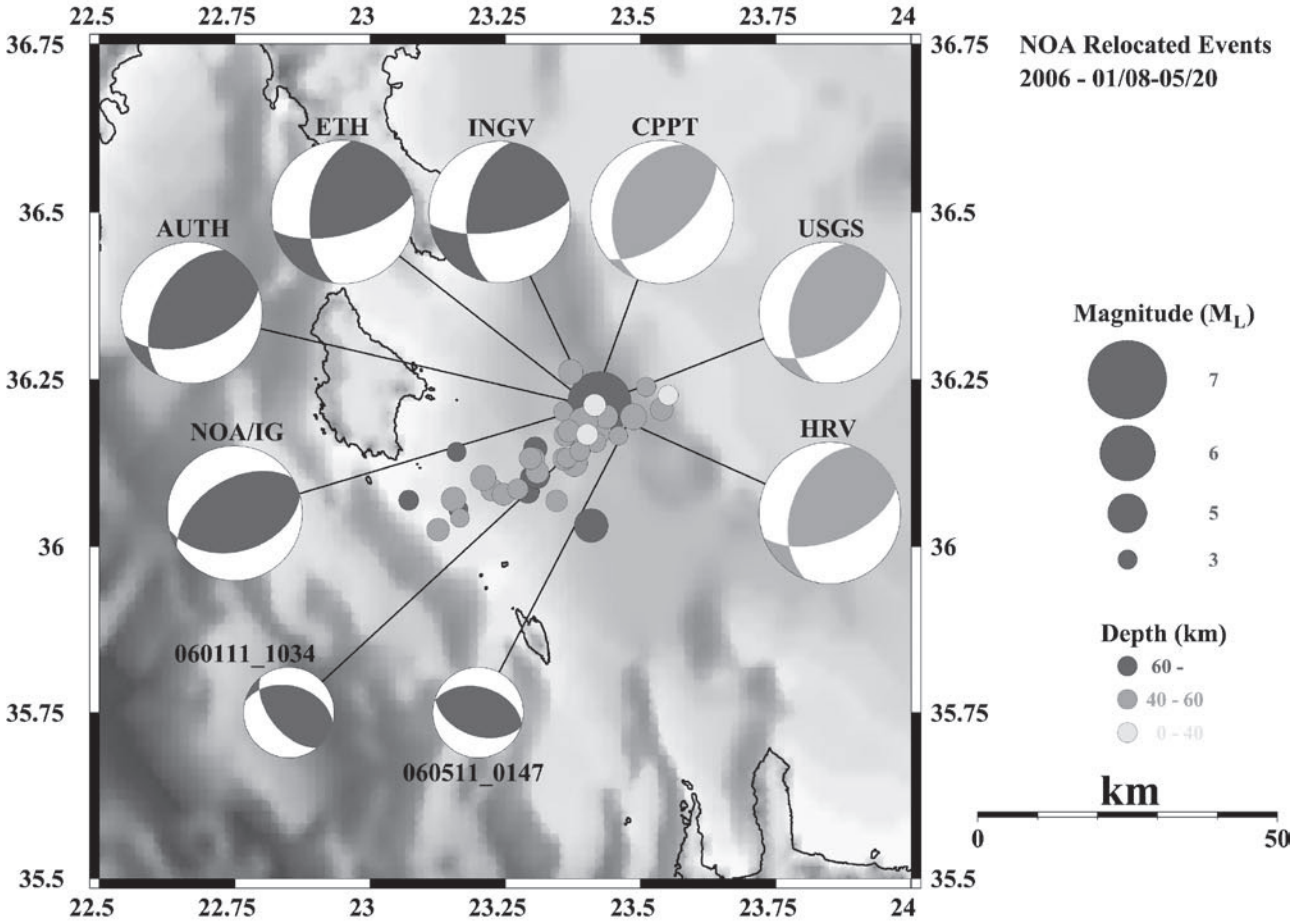

▲ **Figure 3.** Map showing the distribution of epicenters for the mainshock of the Kythira earthquake and its aftershocks. The circle size is proportional to the local magnitude of each event, according to the scale shown at the right side of the plot. In a similar way, the focal depth follows the color scale shown at the right side. All available moment tensor solutions for the mainshock and two of its aftershocks also are plotted (HRV: Harvard CMT, USGS: US Geological Survey, CPPT: French Polynesia Geophysical Laboratory, INGV: Italian National Institute for Geophysics and Volcanology, ETH: Swiss Seismological Service, AUTH: Aristotle University of Thessaloniki, NOAIG: National Observatory of Athens Institute of Geodynamics). For more details see table 2.

TABLE 2
Moment tensor solutions included in the present study

Agency	Depth (km)	M_w	Moment	Plane 1 (ϕ, δ, λ)		
Main Shock (2006 01 08, 11:34, 23.41°E, 36.21°N)						
Regional						
AUTH	64	6.7	1.300E+26 dyn*cm	71	52	120
ETH	55	6.8	0.173E+27 dyn*cm	187	52	33
INGV	79	6.7	1.400E+26 dyn*cm	189	52	29
NOAIG	100	6.4	0.386E+26 dyn*cm	239	49	79
Teleseismic						
HRV	61	6.7	1.500E+26 dyn*cm	200	44	50
USGS	66	6.7	1.300E+19 N*m	193	43	59
CPPT	56	6.8	1.700E+19 N*m	200	33	65
Aftershock (2006 01 11, 10:34, 23.41°E, 36.17°N)						
NOAIG	45	4.3	0.275E+23 dyn*cm	141	56	113
Aftershock (2006 05 11, 01:47, 23.48°E, 36.19°N)						
NOAIG	75	4.3	0.284E+23 dyn*cm	108	47	92

Table 3 gives a summary of the strong-motion instrument types, site geological conditions, and PGA values registered during the Kythira mainshock. We note that although some instruments were in operation, they were not triggered, so PGA at these stations is estimated to be lower than the triggering threshold of the instrument (6–10 mg). Figure 4 shows some representative examples of available recordings that reveal the relatively long duration of the strong motion (>30 s). On the other hand, the corresponding response spectra appear to be dominated by long-period (up to 2.5 s) strong ground motion

TABLE 3
Summary of the strong-motion instruments (type, site, local geology) and the peak ground acceleration values recorded due to the Kythira (Greece) earthquake of 8 January 2006

Type	Code	Site	Lat N	Lon E	PGA mg	Epic. Dist. (km)	Local Geology
ETNA[2]	KYT1	POTAMOS	36.30	22.97	120	33	Limestone, wethered limestone
QDR[2]	ANS1	AG. NIKOLAOS	36.472	23.101	130	42	Sandstones and sands
QDR[2]	CHN1	CHANIA	35.517	24.021	41	93	Recent deposits
QDR[2]	KRN1	KORONI	36.82	21.961	24	144	Alluvial deposits, Cretaceous Limestone
QDR[2]	HER1	IRAKLIO	35.318	25.102	50	183	Clayey mud, Clayey marls
QDR[4]	ELLA	ELLINIKO	37.89	23.74	< 8	189	Recent deposits
A800[1]	ATHC	AMPHITHEA	37.931	23.698	17	194	Sandy clay, pebbles
ETNA[3]	KERA	KERATSINI	37.96	23.61	16	195	Tertiary deposits
A800[1]	KORA	KORINTHOS	37.93	22.93	23	196	Recent deposits
A800[1]	RNTA	RENTIS	37.96	23.67	25	196	Deposits of sand, silt, clay and pebbles
QDR[1]	DFNA	DAFNI	37.95	23.74	< 6	196	Recent deposits
A800[4]	FIXA	SYGROU-FIX	37.960	23.730	6	197	Athenian Schist
A900[1]	NOAA	ATHENS- THISSIO	37.973	23.718	6	198	Limestone
A800[4]	SGMA	SYNTAGMA	37.98	23.74	<8	199	Athenian schist
A800[4]	SGMB	SYNTAGMA	37.98	23.74	<6	199	Athenian schist
A800[1]	DMKA	DIMOKRITOS	38.00	23.82	13	201	Metamorphosed schist
A800[4]	SPLB	SEPOLIA	38.00	23.71	28	201	Silty clay, conglomerate, sandy siltstone
QDR[4]	AGLA	AIGALEO	37.99	23.66	< 6	201	Weathered limestone
A900[1]	ATHA	N.PSYCHIKO	38.001	23.774	11	202	Tertiary deposits
A800[4]	PNTA	ETHNIKI AMYNA	38.000	23.790	10	202	Tertiary deposits
QDR[4]	AGAA	AGIOS ANTONIOS	38.01	23.69	< 8	202	Recent deposits
A800[1]	PRSA	PERISTERI	38.02	23.69	20	204	Recent deposits
QDR[1]	ILIA	ILION	38.03	23.70	< 8	204	Recent deposits
QDR[1]	KHAA	AGIA PARASKEVI	38.02	23.82	< 6	205	Recent deposits
A800[1]	RFNA	RAFINA	38.02	23.97	< 8	208	Tertiary deposits, Limestone
GURALP[2]	NAX1	NAXOS	37.101	25.374	3	208	-
A800[1]	XLCA	XYLOKASTRO	38.08	22.63	26	219	Recent deposits
A800[1]	THVC	THIVA	38.320	23.318	13	235	Cemented Silty Clay, Cemented Conglomerate
ETNA[3]	ALVA	ALIVERI	38.39	24.05	5	249	Tertiary deposits
QDR[1]	CHAA	CHALKIS	38.47	23.62	< 10	252	Recent deposits
K2[2]	HAL1	CHALKIS	38.47	23.62	7	255	Recent deposits
A800[1]	AIGA	AIGIO	38.25	22.03	< 6	258	Clayey Sands, Sandgravels & rubbles, Silty Sand, conglomerate
A800[1]	PATB	PATRA	38.24	21.72	12	271	Alluvium deposits
A800[1]	ATLA	ATALANTI	38.653	22.999	< 8	274	Clays, sands, gravels
A800[1]	ISTA	ISTIAEA	38.951	23.152	< 8	306	Tertiary deposits

1. Instrument operated by NOAIG
2. Instrument operated by ITSAK
3. Instrument operated by PPC
4. Instrument operated by NOAIG and AM

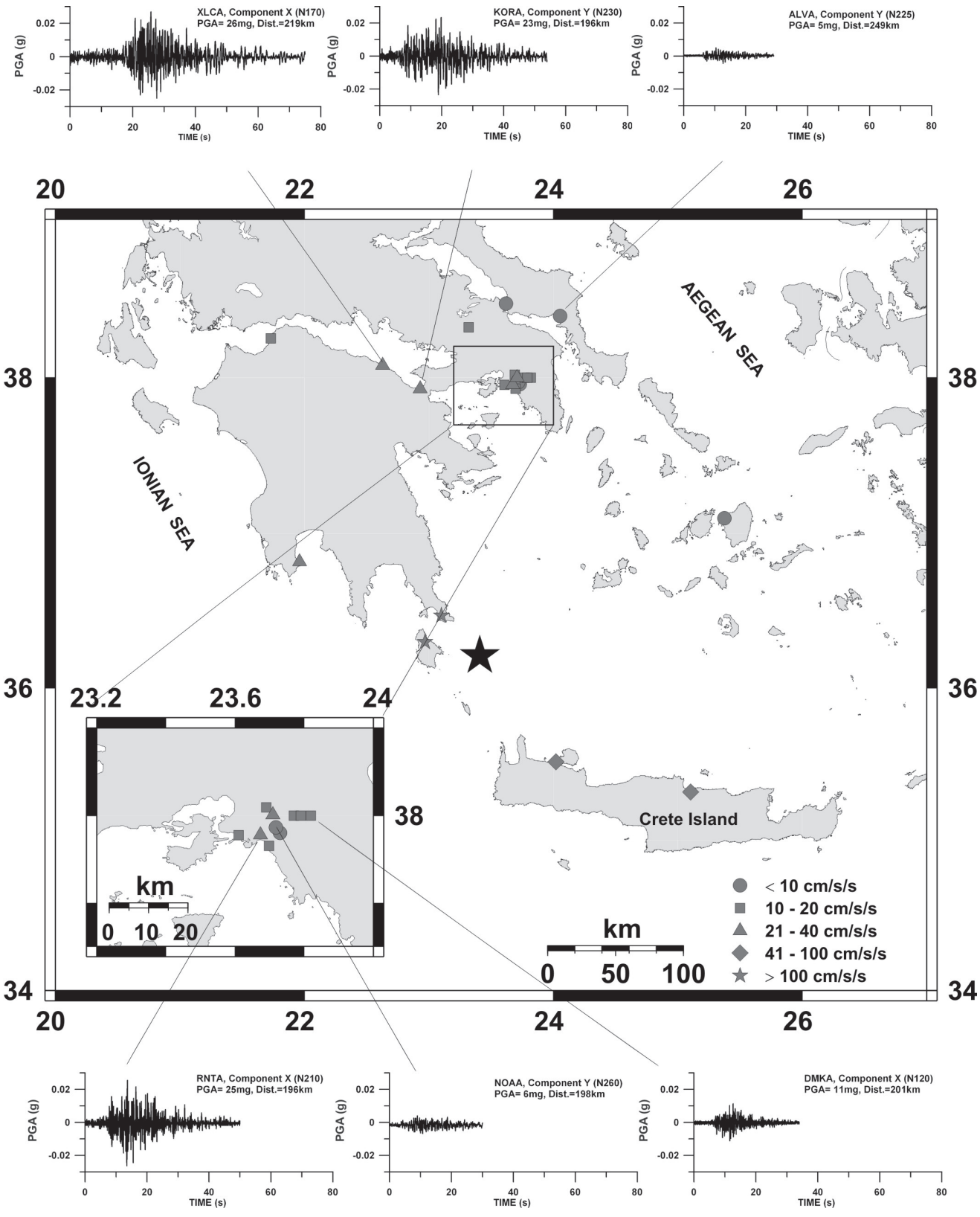

▲ **Figure 4.** Examples of strong ground motion recorded during the Kythira earthquake by a number of instruments in and around the Athens metropolitan area. The star represents the epicenter of the mainshock and the different symbols indicate PGA values registered at those locations (see scale at lower right).

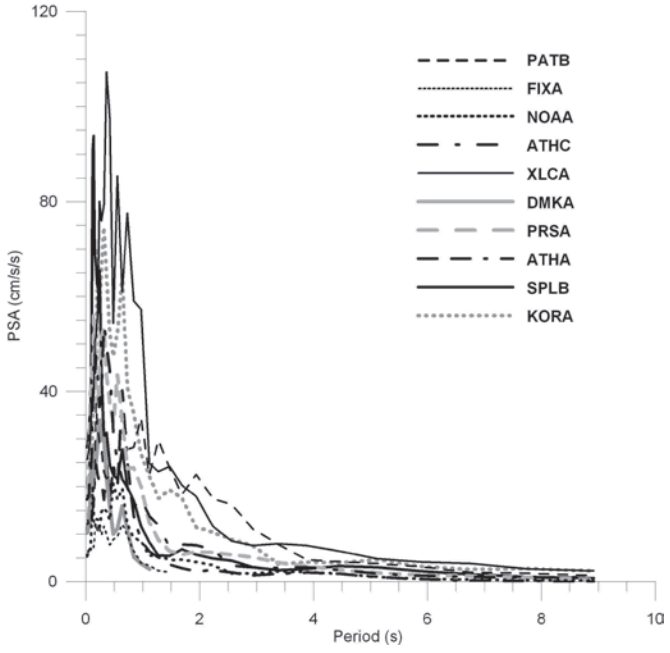

▲ **Figure 5.** Diagram showing the response spectra corresponding to strong ground motion recordings of the Kythira event at several different sites around the Athens metropolitan area (for more information about each particular location/site, see table 3).

(figure 5). This is in contrast to observations of strong ground motion recorded during shallow near-field events, where the dominant periods are usually shorter than 0.5 s (Theodulidis *et al.* 2004).

To check the influence of the local geological conditions on the observed PGA values, we first grouped station local geology into different soil categories based on the Greek National Seismic Code. Then we estimated the fall-off of PGA values versus epicentral distance for both rock and soil using two empirical relationships suggested by Youngs *et al.* (1997) for subduction-zone (interface and intraslab) earthquakes. Figure 6 shows the PGA values observed at different types of soil as a function of epicentral distance, compared with the predicted rock and soil curves. Even though most stations lie on soils C (weathered material of medium quality) or D (alluvial deposits), the PGA values are lower than those predicted for rock by the relationship of Youngs *et al.* (1997). This could be attributed either to a higher absorption of energy for intermediate depth events along the Hellenic arc or to inconsistencies in the soil classification scheme utilized by the Greek National Seismic Code.

MACROSEISMIC OBSERVATIONS AND INTENSITY ATTENUATION

The collection of macroseismic observations by NOAIG started shortly after its establishment (1893) and follows generally the same procedure. After a moderate or strong earthquake, a printed questionnaire is sent to the local authorities of selected (according to spatial distribution and population) towns and villages. The completed questionnaires are then evaluated fol-

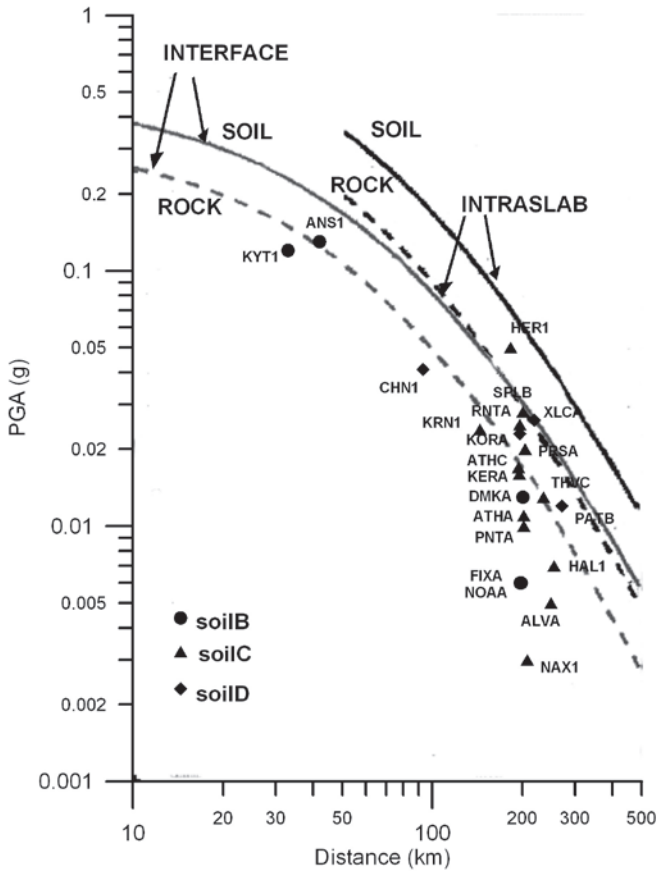

▲ **Figure 6.** Diagram showing the distribution of all available PGA values registered during the Kythira mainshock versus epicentral distance. Each site has been classified into three different soil types described by the Greek National Seismic Code. The curves that represent the predicted fall-off of PGA values versus distance for rock/soil local geology either for interface or intraslab earthquakes (Youngs *et al.* 1997) are also shown for reference.

lowing a Greek version of the Modified Mercalli Intensity scale (Papaioannou 1984) and the macroseismic data are then published in the monthly bulletins of the NOAIG.

According to first reports, the Kythira earthquake was felt in most parts of Greece, so questionnaires were sent to all the prefectures of the country. In total 666 questionnaires were sent and 304 were completed and returned by the local authorities. The reported answers clearly indicate that despite its large magnitude, the earthquake did not cause serious damage owing to its large focal depth. For example, at Potamos village (on Kythira island) situated only 35 km from the epicenter, the reported intensity was only V+. At the village of Mitata, where the most serious damage occurred (intensity VII+), local site amplifications appear to have been responsible for the relatively severe shaking, since similar observations also were reported after another intermediate-depth earthquake in 1903. The macroseismic data also indicate the considerably long duration of the shock, which was felt at epicentral distances between 100 and 200 km with intensities IV–V (see also http://gein.noa.gr [strong earthquakes]). These observations are consistent with

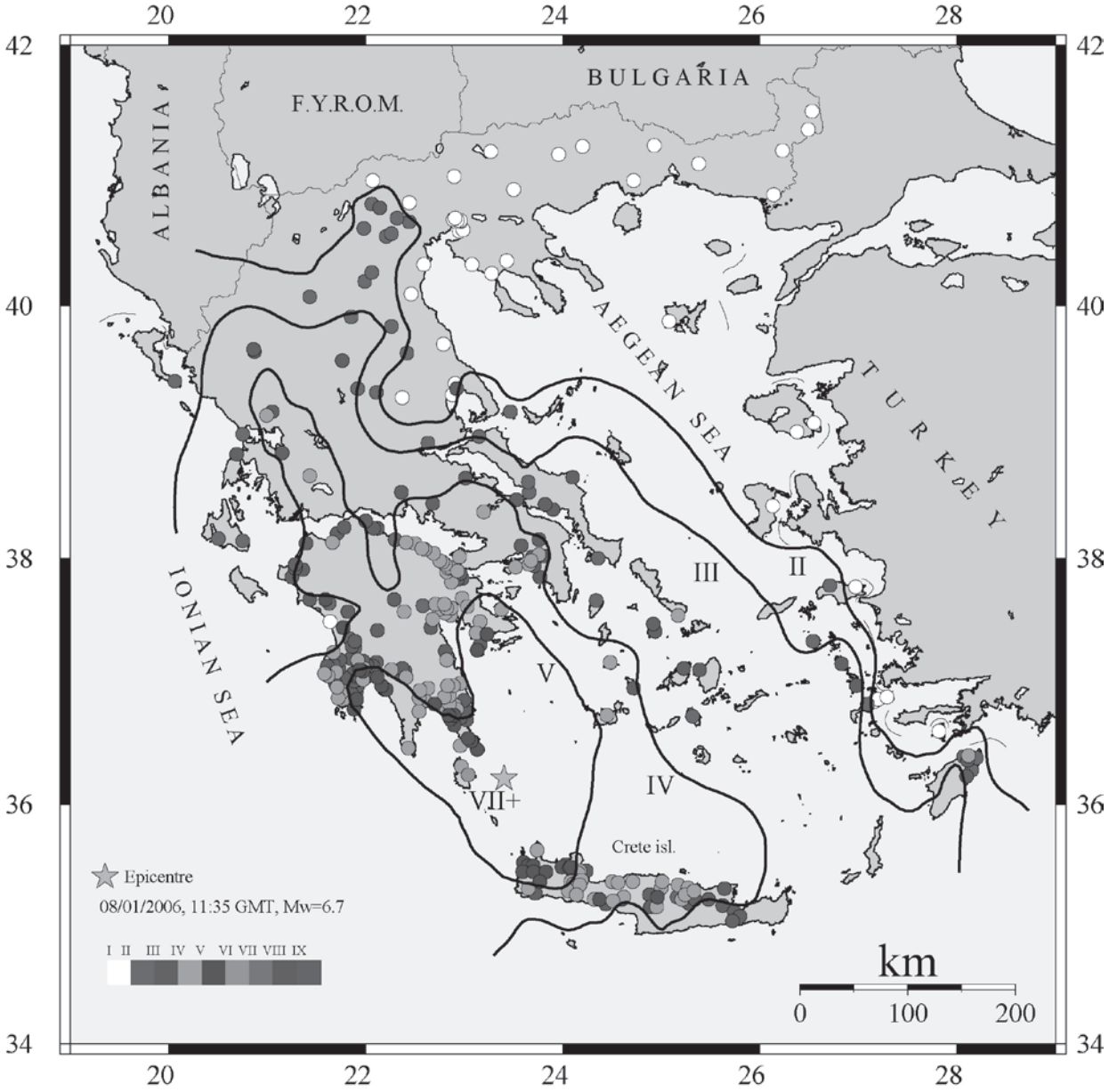

▲ **Figure 7.** Map containing the drawn isoseismal curves using the kriging method of Schenkova *et al.* (2006). Filled circles represent all available macroseismic reports, and their color follows the intensity scale shown at the lower left of the map.

the strong-motion recordings and response spectra presented earlier.

Figure 7 shows a map of the isoseismal curves derived from the macroseismic data following the methodology of Schenkova *et al.* (2006), based on a kriging method. It is evident that the earthquake was not felt at the eastern parts of northern Greece (Macedonia and Thrace) and at the islands close to the coast of Asia Minor (Lesvos, Chios, Samos, and Kos). In contrast, intensities of III+ or greater were reported in the forearc region of the Hellenic arc (*e.g.,* the islands of Crete and Rhodes. This asymmetric distribution of intensities in either side of the arc after an intermediate-depth event has been noted previously by a number of authors (see, for example, Ambraseys and Adams 1998 and references therein). The most likely explanation for these observations is the attenuation of seismic waves (especially that of shear waves) after their passage through the partially melted asthenospheric wedge above the subduction zone (Oliver and Isacks 1967). In terms of a quantitative assessment of intensity attenuation versus epicentral distance, our observations are consistent with the empirical relationship previously published by Papazachos and Papazachou (1997) for intermediate depth earthquakes in Greece (figure 8).

CONCLUDING REMARKS

The Kythira earthquake of 8 January 2006 is (to the best of the authors' knowledge) the first intermediate-depth event that occurred in the Hellenic arc for which a wealth of instrumental

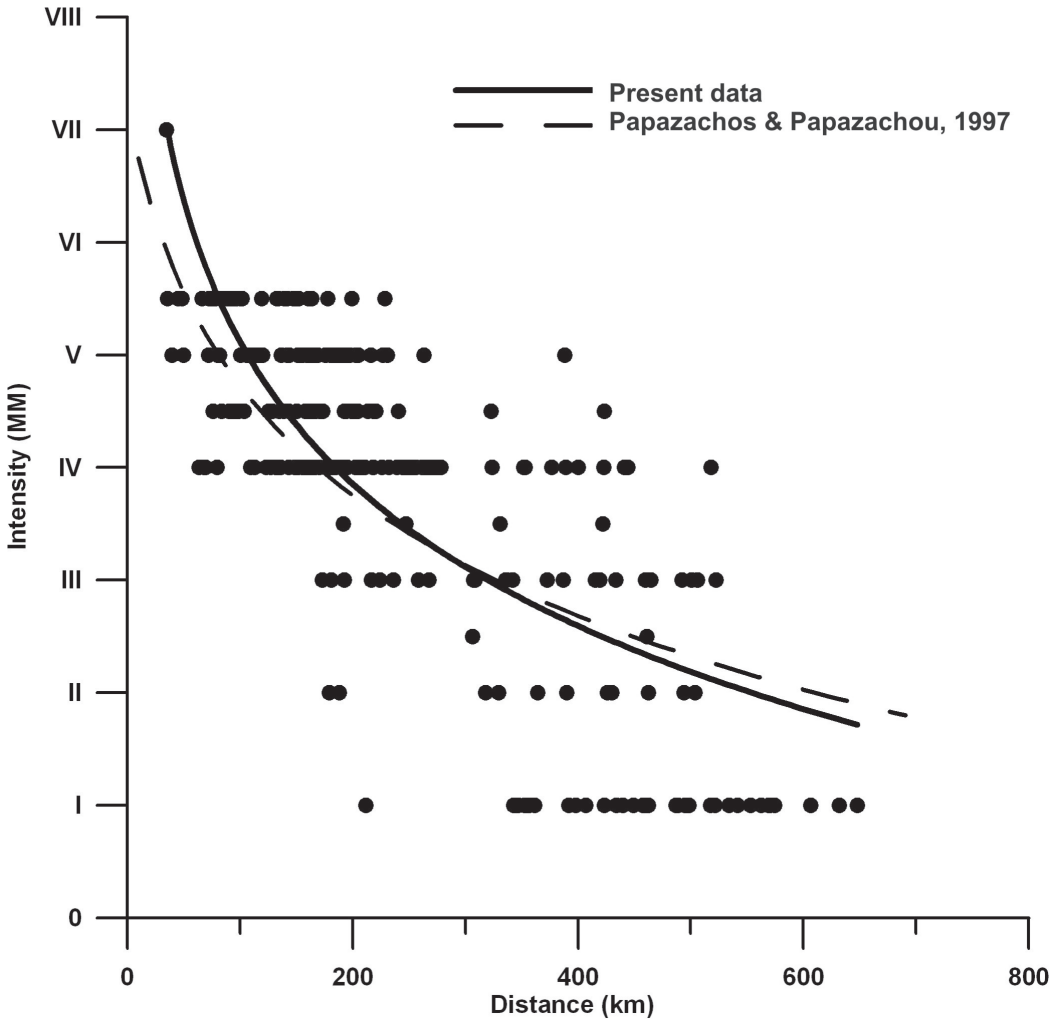

▲ **Figure 8.** Distribution of intensity values reported in the Greek region after the Kythira event versus epicentral distance. Also shown is the curve that better fits the present data and the one published by Papazachos and Papazachou (1997). The latter has been calculated for M 6.7.

or other observations is available. Seismological data from the HL network allowed the location not only of the mainshock but also of several of its aftershocks, delineating the seismogenic structure responsible for this sequence. The determination of focal mechanisms using waveform inversion methods also revealed the presence of thrust-faulting motion that may indicate the existence of lateral compressional stresses at that part of the Hellenic subduction zone. This dataset can be further used to obtain precise relative locations and a model for the slip distribution of the mainshock. The results thus obtained can be combined with current geochemical and thermal models of slab dehydration processes (*e.g.,* Hacker *et al.* 2003) for the purpose of elucidating the generation mechanism of intermediate-depth seismicity.

It was also the first time that an intermediate-depth event triggered a large number of strong-motion instruments at different distances, azimuths, and soil conditions within the Greek region. The strong attenuation (especially in the backarc area) and the long duration of the recordings are consistent with the macroseismic observations collected after the event. An interesting result stemming from the strong-motion data is the common response of different soil categories to the shaking induced by the earthquake. The behavior of soils during large intermediate-depth events and their classification should therefore be reexamined within the frame of the Greek National Seismic Code. Also, the relatively long period (up to 2.5 s) energy that dominated the response spectra clearly shows that intermediate-depth earthquakes originating along the Hellenic arc have the potential to cause damage at large distances inside the forearc area. This conclusion is supported by high intensity values observed in lower Egypt and especially in the Cairo metropolitan area after such events (Ambraseys 2001).

ACKNOWLEDGMENTS

The Public Power Corporation and the Attiko Metro S.A. are acknowledged for providing the strong-motion records from their networks. The present work was partly supported by

NATO Collaborative Linkage Grant 979849. We thank Dr. S. E. Hough for her comments and improvements to the original manuscript.

REFERENCES

Ambraseys, N. N. (2001). Far-field effects of Eastern Mediterranean earthquakes in Lower Egypt, *Journal of Seismology* **5**, 263–268.

Ambraseys, N. N., and R. D. Adams (1998). The Rhodes earthquake of 26 June 1926, *Journal of Seismology* **2**, 267–292.

Hacker, B. R., S. M. Peacock, G. A. Abers, and S. D. Holloway (2003). Subduction factory 2. Are intermediate depth earthquakes in subducting slabs linked to metamorphic dehydration reactions? *Journal of Geophysical Research* **108**, 2030.

Kalogeras, I., and G. N. Stavrakakis (2001). *The Athens, Greece September 7, 1999 Earthquake: Strong Motion Data Processing (7/9/1999–31/3/2000)*, National Observatory of Athens, Institute of Geodynamics publication no. 14 (CD-ROM with user's manual).

Karakostas, C., T. Makarios, V. Lekidis, T. Salonikios, S. Sous, K. Makra, A. Anastasiadis, N. Klimis, P. Dimitriou, B. Margaris, C. Papaioannou, N. Theodulidis, and A. Savvaidis (2006). The Kythira earthquake of January 8, 2006: Preliminary report on strong motion data, geotechnical and structural damage, http://www.eeri.org/lfe/pdf/greece_kythira_ITSAK.pdf.

Klein, F. (2002). *User's Guide to Hypoinverse 2000, a FORTRAN Program to Solve for Earthquake Locations and Magnitudes*, USGS Open File Report 02-171.

LePichon, X., N. Chamot-Rooke, S. Lallemant, R. Noomen, and G. Veis (1995). Geodetic determination of the kinematics of central Greece with respect to Europe: Implication for Eastern Mediterranean tectonics, *Journal of Geophysical Research* **100**, 12,675–12,690.

Lyberis, N., J. Angelier, E. Barrier, and S. Lallemant (1982). Active deformation of a segment of arc: The strait of Kythira, Hellenic arc, Greece, *Journal of Structural Geology* **4**, 299–311.

McClusky *et al.* (2000). Global Positioning System constraints on plate kinematic and dynamics in the Eastern Mediterranean and Caucasus, *Journal of Geophysical Research* **105**, 5,695–5,719.

McKenzie, D. (1972). Active tectonics of the Mediterranean region, *Geophysical Journal of the Royal Astronomical Society* **30**, 109–185.

McKenzie, D. (1978). Active tectonics of the Alpine-Himalayan belt: The Aegean Sea and surrounding regions, *Geophysical Journal of the Royal Astronomical Society* **55**, 217–254.

Melis, N. S., and K. I. Konstantinou (2006). Real-time seismic monitoring in the Greek region: An example from the 17 October 2005, East Aegean Sea earthquake sequence, *Seismological Research Letters* **77**, 364–370.

Nyst, W., and W. Thatcher (2004). New constraints on the active tectonic deformation of the Aegean, *Journal of Geophysical Research* **109**, 11,406.

Oliver, J., and B. Isacks (1967). Deep earthquake zones, anomalous structure in the upper mantle and the lithosphere, *Journal of Geophysical Research* **72**, 4,259–4,275.

Papaioannou, C. A. (1984). Attenuation of seismic intensities and seismic hazard in the area of Greece. Ph.D. thesis, University of Thessaloniki (in Greek).

Papazachos, C. B., and G. Nolet (1997). P and S velocity structure of the Hellenic area obtained by robust nonlinear inversion of travel times, *Journal of Geophysical Research* **102**, 8,349–8,367.

Papazachos, B. C., and K. Papazachou (1997). *The Earthquakes of Greece*. Thessaloniki, Greece: Ziti Editions, , 304 pp.

Randall, G. E., C. J. Ammon, and T. J. Owen (1995). Moment tensor estimation using regional seismograms from a Tibetan Plateau portable network deployment, *Geophysical Research Letters* **22**, 1,665–1,668.

Schenkova, Z., V. Schenk, I. Kalogeras, R. Pichl, P. Kottnauer, C. Papatsimpa, and G. Panopoulou (2006). Isoseismal maps drawing by the kriging method, *Journal of Seismology*, in press.

Theodulidis, N., I. Kalogeras, C. Papazachos, V. Karastathis, B. Margaris, C. Papaioannou, and A. Skarlatoudis (2004). HEAD 1.0: A unified Hellenic Accelerogram Database, *Seismological Research Letters* **75**, 36–45.

Youngs, R. R., S. J. Chiou, W. J. Silva, and J. R. Humphrey (1997). Strong ground motion attenuation relationships for subduction zone earthquakes, *Seismological Research Letters* **68**, 58–73.

Institute of Geodynamics
National Observatory of Athens
POB 20048 118 10
Athens, Greece
nmelis@gein.noa.gr
(N.S.M.)